FDTD Analysis of Phased Array Antennas

Gregory M. Turner, *Member, IEEE,* and Christos Christodoulou, *Senior Member, IEEE*

***Abstract*—This work presents a new application of the finite-difference time-domain (FDTD) method to the generalized analysis of phased array antennas. The generality of the FDTD method brings important advantages to the phased array antenna analysis problem, allowing the modeling of complex conductor and dielectric geometries with relative ease. Additionally, a new broad-band FDTD periodic boundary condition is developed which allows the array problem to be simplified to a periodic unit cell computational domain. This hybrid frequency/time-domain periodic boundary condition enables solution of the periodic phased array problem for arbitrary scan conditions in a broad-band fashion. The new method is applied to waveguide and stacked microstrip antenna arrays and the numerical results are compared to experimental or analytic solutions, demonstrating the validity and utility of this method.**

***Index Terms*— FDTD, microstrip antennas, phased arrays, stacked arrays.**

I. Introduction

THE ADVANCEMENT of enabling technologies has thrust phased array antennas to the forefront of the antenna industry, as the features of electronic steerability, light weight, and conformability make phased arrays the antenna of choice for many applications. This emergence has resulted in an increased emphasis on numerical methods for array radiating element design. Accurate numerical modeling techniques are particularly important for array applications due to the cost and effort associated with breadboard and development model fabrication and test. Desirable features of these methods include the generality required to model a wide range of radiator types and the ability to accurately model array environment effects on performance of the individual radiating elements.

The predominant technique for array radiating element analysis is the method of moments (MoM). The MoM is readily adapted to the infinite periodic array case and has been proven successful in treating many such problems [1]–[3]. The MoM use of analytic Green's functions provides a technique that is well suited to problems consisting of infinite dielectric layers and thin conductors as is the case for many microstrip array antennas and frequency selective surfaces. As radiating element geometries become more complex, with laterally inhomogenous dielectric features and three-dimensional (3-D) conductor geometries, the MoM method is less effective and a more general approach is required. The finite-element method (FEM) is one example of a more general approach that is capable of modeling arbitrary radiator geometries and has been effectively combined in hybrid techniques for infinite array analysis [4], [5].

The finite-difference time-domain (FDTD) method provides a completely general formulation. Originally introduced by Yee [6], the FDTD method has been applied to a wide variety of problems. Recent advances in FDTD modeling techniques combined with advances in computer technology have expanded the scope, accuracy, and speed of FDTD modeling to the point where it is the preferred method for many problems involving complex 3-D structures. A unique benefit of the FDTD method relative to the MoM and hybrid MoM/FEM techniques is the capability for broad-band transient analysis which can dramatically increase its efficiency as a radiating element design tool.

In this paper, methods for applying the FDTD method to the analysis of infinite periodic array antennas are described. The result is a completely general and highly efficient method for modeling active reflection characteristics of array radiating elements of arbitrary composition. Two examples are provided that validate and demonstrate the utility of this approach. The first compares numerical results to experimentally derived active reflection coefficients for a stacked microstrip patch array. The second example compares numerical results to exact analytic expressions for the active reflection coefficient of the canonical thin walled waveguide array.

II. FDTD Periodic Boundary Conditions

A fundamental simplification for the array radiating element analysis is achieved by assuming the array is of infinite extent along the periodic axes. The infinite array approximation provides an accurate prediction for the majority of centrally located elements in a large array. The computational domain for the infinite array analysis is limited to a unit cell of the array by applying appropriate boundary conditions normal to the periodic axes of the array. The general periodic array geometry is illustrated in Fig. 1.

The well-known Floquet theorem defines the fields associated with this periodic structure as repeating at spatial intervals equivalent to the unit cell dimensions, with time shifts corresponding to the angle of incidence, or scan angle in the case of a phased array, according to

$$\mathrm{E}(x, y, t) = \mathrm{E}\left(x + mD_x, y + nD_y, t + \frac{mD_x}{v_{phx}} + \frac{nD_y}{v_{phy}}\right) \tag{1}$$

where m and n are the periodic cell indexes ranging from $-\infty$ to $+\infty$, D_x and D_y are the unit cell dimensions, and v_{phx} and v_{phy} are the phase velocities along the x and y

Manuscript received November 21, 1997; revised March 16, 1998.

G. M. Turner is with the Harris Corporation, Melbourne, FL 32902 USA.

C. Christodoulou is with the Department of Electrical and Computer Engineering, University of New Mexico, Albuquerque, NM 87131 USA.

Publisher Item Identifier S 0018-926X(99)04772-9.

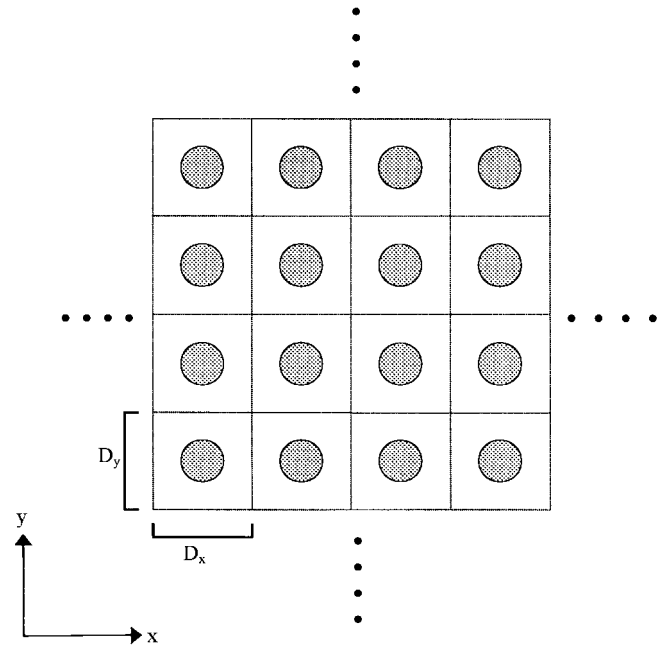

Fig. 1. General periodic array geometry with unit cell dimensions.

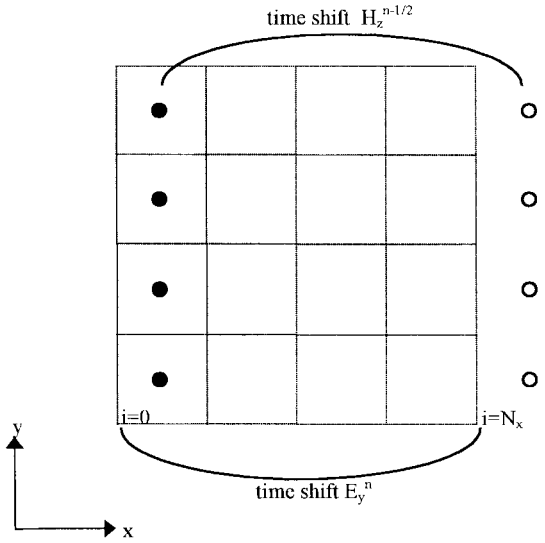

Fig. 2. Illustration of the wrap-around boundary field update at the $+x$ and $-x$ FDTD mesh boundaries.

axis, respectively. The Floquet theorem allows the fields at any position in the periodic structure to be represented by a time-shifted version of the fields within the unit cell. The implication with regard to the FDTD algorithm is that the field values that lie one-half step outside the unit cell FDTD mesh, required for updating boundary field values, can be represented by time-shifting field values from within the unit cell FDTD mesh. This "wrap-around" boundary field update is illustrated in Fig. 2. The tangential electric fields at the periodic boundary can be updated by using magnetic field values located one-half step inside the opposing boundary, with an appropriate time shift, to represent the magnetic field values one-half step outside the local boundary. Tangential electric fields at the opposing boundary are updated by simply performing the time shift and wrap-around operations on the previously updated local boundary fields.

The wrap-around boundary technique was used for FDTD analysis of scattering and radiation from infinitely periodic arrays in [7]. This formulation used a Gaussian pulse excitation to enable broad-band response characterization. This application was limited to the broadside incidence case however, where the wrap-around time shifts are set to zero and FDTD implementation is relatively straightforward. For the more general formulation, the time shifts that are required to be applied to field values as they are wrapped around the FDTD grid present some problems to the standard algorithm. While time delays can be implemented in the FDTD algorithm by storing field values over a series of time steps (at considerable computer memory expense), time advanced field values are also required and are not feasible within the FDTD scheme. In [8], the authors implemented a true time-delay periodic FDTD formulation by extending the computational domain to three unit cells along the periodic axis and using a preliminary subprogram to generate the time advanced fields. This treatment is only an approximation however, and does not provide a true infinite array representation.

A frequency-domain phase shift alternative to the time shift used with the FDTD wrap-around was introduced in [9] and applied to scattering from periodic structures in [10] and [11]. This frequency-domain periodic FDTD method utilized dual computational domains with time harmonic sine and cosine excitations, providing a phasor representation of all field components at all times. The phase shift required for the periodic boundary wrap-around updates was implemented by combining components of the dual computational domains to form a phasor field representation, shifting the phase, and redistributing the components to the sine and cosine based domains. A significant drawback to this approach is that the problem is solved one frequency at a time and the broad-band FDTD capability is not exploited.

In this work, the frequency-domain phase shift periodic boundary methodology is employed to allow arbitrary phased array scan conditions to be modeled. In contrast to the previous examples however, the sine and cosine components are used to modulate Gaussian pulse excitations. The resulting outputs from this formulation can be processed to provide broad-band response information for a fixed-boundary phase shift condition, providing a dramatic increase in efficiency over the previous formulations. Additionally, the dual computational-domain approach is simplified by utilizing complex variables with the real and imaginary components representing the cosine and sine-based time modes.

III. FDTD Implementation

Fig. 3 depicts the general setup for the FDTD array radiating element model. Dimensions of the computational domain in the x and y axis are chosen to correspond to the infinite array unit cell dimensions D_x and D_y. Wrap around periodic boundary conditions are applied to terminate the FDTD mesh on the planes normal to the periodic axes. An absorbing boundary condition is used to terminate the mesh in the $+z$

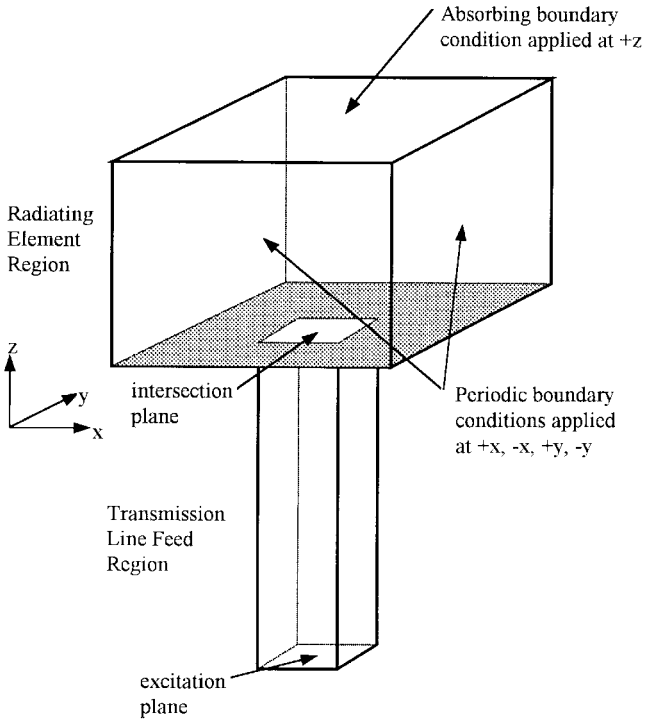

Fig. 3. FDTD model for unit cell of an infinite array.

direction and the $-z$ boundary is typically treated as a perfect electrical conductor to represent a ground plane. A feeding transmission line intersects the radiating element region at the ground plane and extends for some distance where it is terminated at the excitation plane.

A. Excitation and Feed Modeling

The excitation is applied to the FDTD grid by setting the tangential electric field values at the excitation plane according to

$$E_{\text{exc}}(x, y, t) = F(x, y)[\cos(\omega t) + j\,\sin(\omega t)]e^{-((t-t_o)/T)^2}. \tag{2}$$

These field values consist of a complex sinusoid modulating a Gaussian pulse, with spatial variation $F(x, y)$ corresponding to the fundamental transmission line propagation mode (e.g., TEM for coax or TE_{10} for rectangular waveguide). An example of a coaxial feed transmission line FDTD model cross-section is illustrated in Fig. 4, along with the electric field distribution used to approximate the TEM mode. In this example, the coaxial line is modeled using square inner and outer conductors of 2×2 and 6×6 grid cells, respectively. The dielectric constant within the coaxial line is set to provide a 50 Ω impedance.

A start-up delay of $t_o = 2.5$ T is used so that the excitation field values start near zero. Once the pulse is launched into the model and the excitation has decayed to a negligible level ($t = 5$ T is used in this case), the excitation plane is switched to an absorbing boundary to eliminate spurious reflections from the excitation plane. A voltage sampling point is chosen at a location on the transmission line that is relatively close to the radiating element region. The length

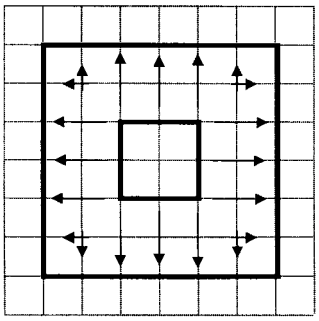

Fig. 4. Coaxial feed transmission line x–y plane discretization and electric field distribution imposed at excitation plane.

of the transmission line is selected such that the excitation can be fully launched into the mesh and the excitation plane converted to an absorbing boundary prior to the arrival of any reflected voltage. Two runs of the FDTD model are required to calculate the reflection coefficient of the radiating element. Voltage sample $V_{\text{reference}}(t)$ is recorded as the model is run with the radiating element portion of the FDTD mesh replaced with an absorbing boundary to simulate the feed transmission line connected to a matched load. Voltage sample $V_{RE}(t)$ is recorded with a full model run, including the radiating element. Since $V_{RE}(t)$ consists of the superposition of the incident and reflected voltages, $V_{\text{reference}}(t)$ must be subtracted to isolate the reflected voltage as shown in (3). The reflection coefficient is then calculated as the ratio of the Fourier transforms of the incident and reflected voltage samples as shown in (4)

$$V'_{RE}(t) = V_{RE}(t) - V_{\text{reference}}(t) \tag{3}$$

$$\Gamma(\omega) = \frac{\Im\{V'_{RE}(t)\}}{\Im\{V_{\text{reference}}(t)\}}. \tag{4}$$

B. Periodic Boundary Conditions

Periodic boundary conditions are applied using the wrap-around technique with a phase shift applied to the complex field variables as they are wrapped around the FDTD mesh. The phase shifts, Ψ_x and Ψ_y, are the steering phases along the x and y axis required to scan the beam in the (θ, ϕ) direction, as defined in the equations

$$\Psi_x = \frac{2\pi D_x}{\lambda}\,\sin\theta\,\cos\phi \tag{5}$$

$$\Psi_y = \frac{2\pi D_y}{\lambda}\,\sin\theta\,\sin\phi. \tag{6}$$

Update equations for tangential electric fields at the $+x$ and $-x$ periodic boundary are provided in (7)–(10). In these equations, superscript n is the time step index and subscripts i, j, and k are the spatial indices corresponding to the x, y, and z axes, respectively, (the 1/2 cell spatial offset between electric and magnetic fields is implicit). The periodic boundaries on the x axis correspond to $i = 0$ and $i = M$

$$\begin{aligned} Ey^{n+1}_{i=M,\,j,\,k} = {} & Ey^{n}_{M,\,j,\,k} \\ & + \frac{\Delta t}{\varepsilon \Delta z}\left(Hx^{n+1/2}_{M,\,j,\,k+1} - Hx^{n+1/2}_{M,\,j,\,k}\right) \\ & - \frac{\Delta t}{\varepsilon \Delta x}\left(e^{-j\Psi x} Hz^{n+1/2}_{1,\,j,\,k} - Hz^{n+1/2}_{M,\,j,\,k}\right) \end{aligned} \tag{7}$$

$$Ez^{n+1}_{i=M,\,j,\,k} = Ez^{n}_{M,\,j,\,k} + \frac{\Delta t}{\varepsilon \Delta x}\left(e^{-j\Psi x} Hy^{n+1/2}_{1,\,j,\,k} - Hy^{n+1/2}_{M,\,j,\,k}\right) - \frac{\Delta t}{\varepsilon \Delta y}\left(Hx^{n+1/2}_{M,\,j+1,\,k} - Hx^{n+1/2}_{M,\,j,\,k}\right) \tag{8}$$

$$Ez^{n+1}_{i=0,\,j,\,k} = e^{j\Psi x} Ez^{n+1}_{M,\,j,\,k} \tag{9}$$

$$Ey^{n+1}_{i=0,\,j,\,k} = e^{j\Psi x} Ey^{n+1}_{M,\,j,\,k}. \tag{10}$$

Special treatment is required for z directed electric field variables at the corners of the FDTD mesh. In this case, a combination wrap around update along both the x and y axis is required as shown in (11) for the $i = M$, $j = N$ corner

$$Ez^{n+1}_{i=M,\,j=N,\,k} = Ez^{n}_{M,\,N,\,k} + \frac{\Delta t}{\varepsilon \Delta x}\left(e^{-j\Psi x} Hy^{n+1/2}_{1,\,N,\,k} - Hy^{n+1/2}_{M,\,N,\,k}\right) - \frac{\Delta t}{\varepsilon \Delta y}\left(e^{-j\Psi y} Hx^{n+1/2}_{M,\,1,\,k} - Hx^{n+1/2}_{M,\,N,\,k}\right). \tag{11}$$

The remaining equations for the y axis periodic boundary at $j = 0$ and $j = N$, and the other grid corners can be similarly adapted from the standard FDTD update equations.

C. Special Treatment for Waveguide Radiating Elements

The implementation described in the preceding paragraphs for broad-band evaluation of radiating elements is applicable to a wide range of common array element types including conformal microstrip patches and vertical printed dipoles or flared notches. Difficulties arise however in applying this same methodology to another important class of array element; the open ended waveguide radiator. The problem stems from the dispersive characteristics of the waveguide feed transmission line, which will distort the Gaussian pulse as it propagates to the aperture and is reflected back, rendering the broad-band transient technique unusable. For waveguide radiating elements, it is necessary to modify the preceding technique to a true frequency-domain, point-by-point technique (note that this treatment is analogous to the original frequency-domain phase shift periodic boundary condition introduced in [9] for the case of scattering from periodic structures). In this case, the dramatic efficiency improvement afforded by the broad-band FDTD method is sacrificed. The benefit of generality of the formulation is maintained, however, and it would be straightforward to model waveguide arrays with complex features including tuning irises, dielectric loads, or radome layers.

The frequency domain method for dispersive elements is implemented by modifying the Gaussian pulse term of the excitation from (2), to a Gaussian ramp-up function that maintains a value of unity after $t = t_o$. Calculation of the reflection coefficient for the frequency domain FDTD is simplified relative to the broad-band time-domain case. Voltage samples are required for one time step only and can be taken at any time after the model reaches a steady state ($t = t_{ss}$). A modified version of (3) and (4) can be used to isolate the reflected voltage and ratio the incident to reflected voltage as shown in (12). Note that the Fourier transform is not required since the time samples are strictly time harmonic

$$\Gamma = \frac{V_{RE}(t_{ss}) - V_{\text{reference}}(t_{ss})}{V_{\text{reference}}(t_{ss})}. \tag{12}$$

D. Array Lattice Considerations

It should be noted that the periodic boundary condition as defined here is specific to a rectangular array lattice. It is the authors contention that this boundary condition can be adapted to a nonrectangular lattice by employing a spatial shift along the periodic boundary as the field variables are wrapped around for the boundary update. This aspect is not explored any further in this work, however, and is left as an area for further investigation.

IV. Numerical Results

In this section, examples of numerical results obtained using the preceding methods are presented. These results validate the use of the FDTD method for determining phased array radiating element active reflection coefficients. The first example is a broad-band analysis of a Ku-band stacked, circular microstrip patch array. The radiating element configuration includes multiple conductor layers and a truncated foam dielectric supporting the parasitic patch. The FDTD numerical results are compared to experimentally derived reflection coefficients from measured coupling coefficients for a 54-element array. The second example is a frequency-domain analysis of the canonical thin walled waveguide array [12]. In this case numerical results are compared to exact analytic expressions. In the waveguide array example, the ability of the FDTD method to accurately model surface wave and grating lobe effects on the active reflection coefficient is demonstrated.

A. Ku-Band Stacked Patch Array

The stacked microstrip patch radiating element consists of a circular patch directly coupled to the center conductor of a coaxial feed line and a second circular patch that is electromagnetically coupled to the direct fed element. The direct fed patch conductor is printed on a thin substrate layer that is continuous throughout the array and the parasitic patch is supported by a relatively thick low dielectric foam layer that is truncated at the perimeter of the patch as shown in Fig. 5. The FDTD model used grid cell dimensions of $\Delta x = \Delta y = 0.287$ mm and $\Delta z = 0.103$ mm. A staircase approximation was used to model the curved edge of the circular patch conductors. A seven-layer perfectly matched layer (PML) absorbing boundary [13] was used to terminate the $+z$ wall of the FDTD mesh. The feed transmission line was modeled as a square TEM line as described previously and illustrated in Fig. 4.

The experimental data used to compare with the FDTD numerical results was derived from measured mutual coupling coefficients for a 54-element array arranged in a rectangular lattice (six rows, nine columns). A photograph of the experimental model is provided in Fig. 6. Coupling coefficients from a centrally located element (fifth column, third row) to all of

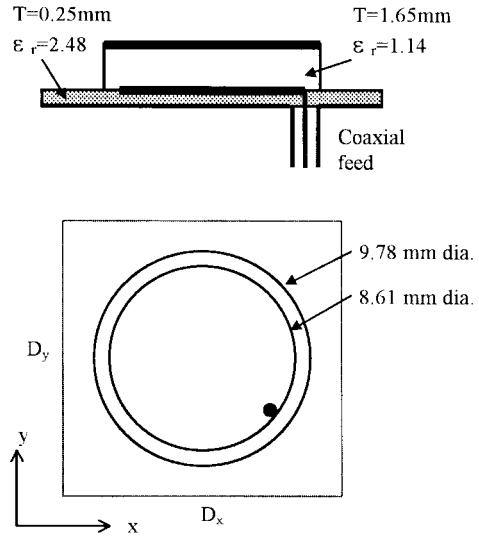

Fig. 5. Stacked microstrip patch configuration, $D_x = 16.51$ mm, $D_y = 19.05$ mm.

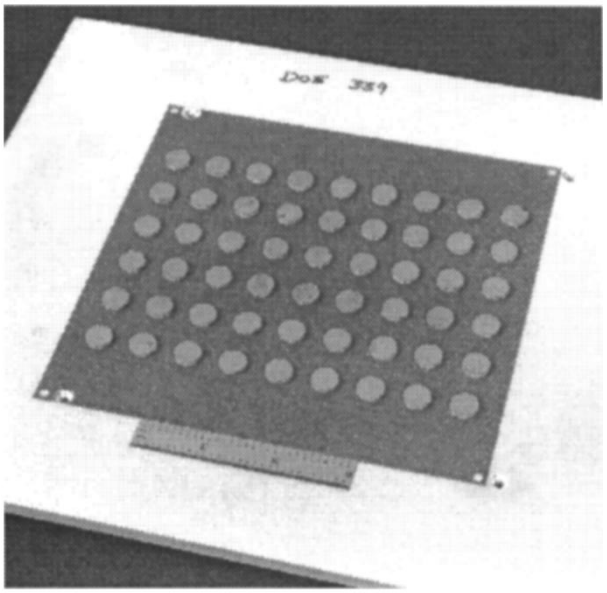

Fig. 6. Stacked microstrip patch array experimental model.

the other elements in the array were measured using a network analyzer. The active reflection was then calculated by summing the measured coupling coefficients with an appropriate phase shift according to the scan angle and element location in the array according to

$$\Gamma = \sum_{i=1}^{9} \sum_{k=1}^{6} C_{ik}^{53} e^{-j((i-5)\Psi_x + (k-3)\Psi_y)} \tag{13}$$

where C_{ik}^{53} is the coupling coefficient from the element in the fifth column, third row to the element in the ith column, kth row, and Ψ_x, Ψ_y are the scan dependent steering phases defined in (5) and (6). In general, this type of experimental method is subject to error due to the finite size of the array. In this case, the coupling to elements as close as three cells away are approximately 30 dB below the dominant self-coupling term, indicating a reasonable approximation to the infinite array environment.

Broad-band numerical results for the Ku-band stacked patch array are compared to experimentally derived active reflection coefficients in Figs. 7 and 8. Fig. 7 shows magnitude and phase of the active reflection coefficient as a function of frequency for the broadside scan condition ($\Psi_x = \Psi_y = 0$). Fig. 8 provides a contour plot of the active reflection coefficient as a function of frequency and steering phase along the x axis. The contour plot of Fig. 8 exemplifies the efficiency afforded by the broad-band FDTD method as all of this data was generated with ten runs of the broad-band FDTD model. In both cases there is good agreement between the numerical and experimental results. Each run took approximately 3 h of CPU time on a Sun Ultra2 computer server.

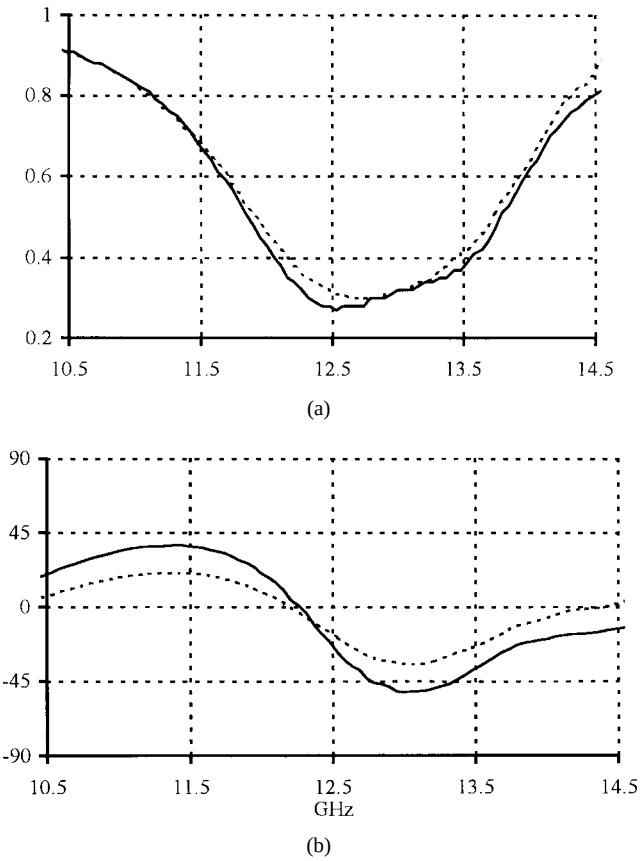

Fig. 7. Broad-band active reflection coefficient for stacked patch array: (a) magnitude and (b) phase: solid—experimental, dashed—FDTD.

B. Thin-Walled Waveguide Array

For the second example, the active reflection coefficient of an infinite waveguide array was determined using FDTD. The waveguide array elements mandated the use of the single frequency version of the FDTD array technique. Numerical results were compared to exact analytic expressions from [12]. The canonical thin-walled waveguide array consists of square waveguide apertures, of dimension 0.56λ, separated by infinitesimally thin walls. The FDTD model for the waveguide array used 24 cells along the x and y axis. Along the z axis, the FDTD grid used 100 cells for the open radiating

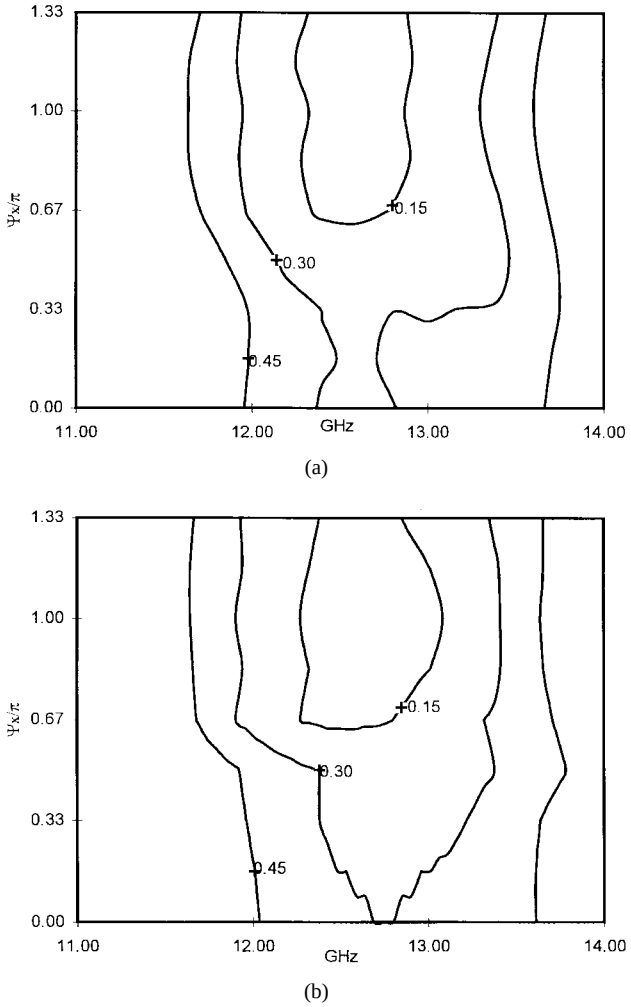

Fig. 8. FDTD active reflection coefficient contour for stacked patch array: (a) experimental and (b) FDTD.

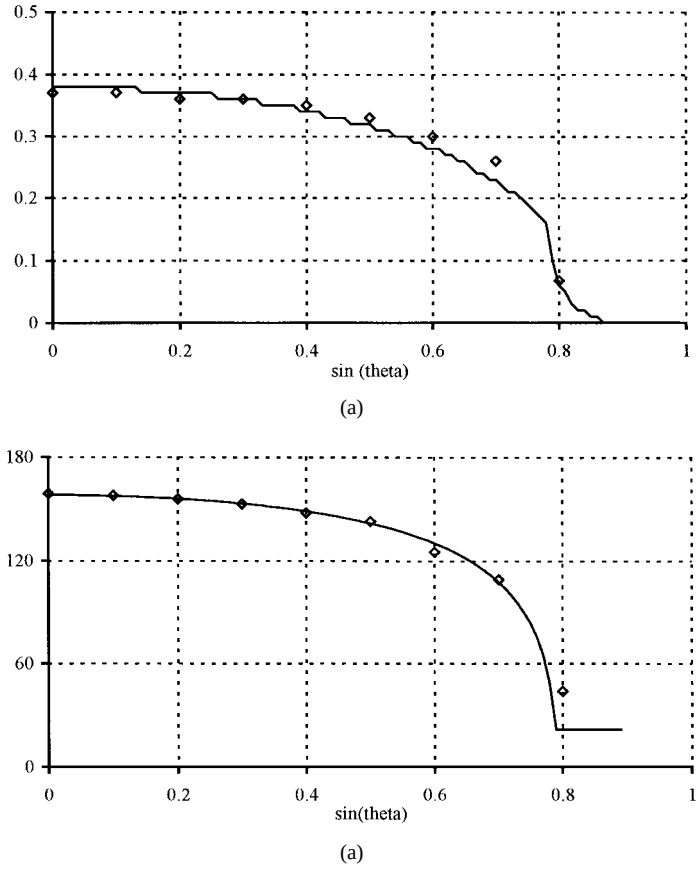

Fig. 9. Active reflection coefficient versus H-plane scan for waveguide array: (a) magnitude and (b) phase: — experimental and ◇ FDTD.

element portion of the model, and 800 cells to represent the feeding waveguide transmission line. A y directed electric field corresponding to the TE_{10} waveguide mode was imposed on the excitation plane at the end of the feed transmission line. A ten-cell PML absorbing boundary was used to terminate the FDTD mesh at the $+z$ boundary. The efficiency of the FDTD technique was significantly reduced in this example due to the number of grid cells used to model the waveguide feed in the x–y plane and due to the use of the single frequency FDTD method. Computer run time was approximately 6 h on a Sun Ultra2 computer server for each scan condition.

Two scan conditions were considered for the thin walled waveguide array. The first condition is an H-plane scan along the x–z plane such that $\Psi_x = 11.22 \sin\theta$ and $\Psi_y = 0$. The second condition is described in [12] as the quasi E-plane scan where the array is scanned in the y–z plane with perfect electric walls placed at the x axis periodic boundaries such that $\Psi_x = \pi$ and $\Psi_y = 11.22 \sin\theta$. The quasi E-plane scan condition, which was selected because it can be solved analytically, results in two beams equally displaced from the y–z plane that scan parallel to the E-plane. Numerical results for the H-plane and quasi E-plane scan case are compared to the exact analytic expressions for active reflection coefficient in Figs. 9 and 10, respectively. Good agreement was obtained for both of these scan conditions including the discontinuities resulting from the introduction of a grating lobe for the H-plane scan case (at $\sin\theta = 0.8$ in Fig. 9) and surface wave propagation for the quasi E-plane scan case (at $\sin\theta = 0.5$ in Fig. 10).

V. Conclusions

In this paper we have presented techniques for applying the FDTD method to the analysis of radiating element active reflection characteristics for phased array antennas. The key to this implementation is the development of periodic boundary conditions that can be applied within the FDTD algorithm. The resulting method provides important advantages over other available methods in its ability to model radiators of arbitrary conductor configuration and dielectric homogeneity coupled with unprecedented efficiency for this type of analysis in most cases due to the inherent broad-band nature of the FDTD method. Two examples were provided that validated and demonstrated the utility of this technique.

One obvious area for future improvements to this method is optimization to reduce the relatively large CPU times required for the solutions. One aspect of these models that drives CPU time is the high resolution required in the FDTD grid to model the fine physical features of the antenna, in particular the coaxial feed for the stacked patch example. Several techniques involving nonuniform grids or subcell grids

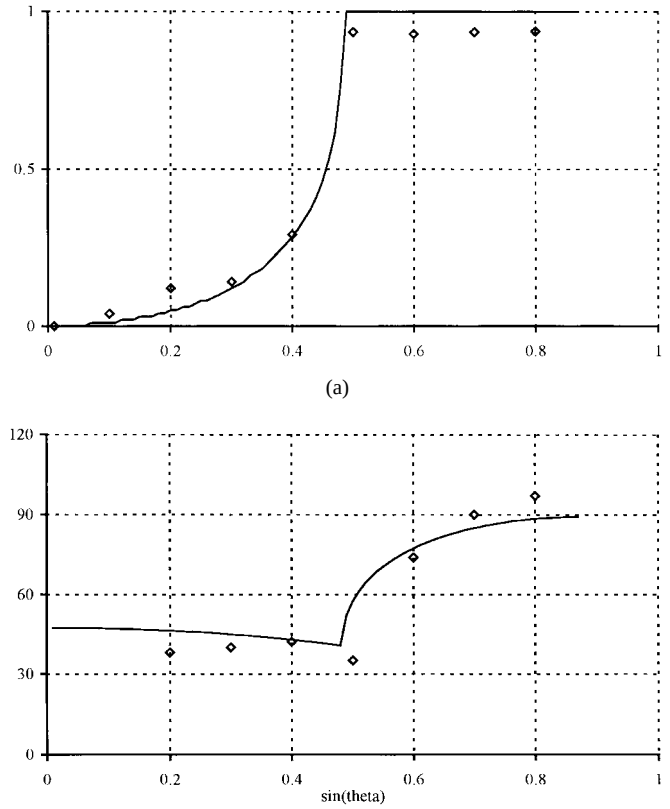

Fig. 10. Active reflection coefficient versus Quasi E-plane scan for waveguide array: (a) magnitude and (b) phase: — experimental and ♢ FDTD.

have been described in the literature that should provide an effective improvement in this regard. A second factor that drives CPU time is length of the feed transmission line required to fully launch the excitation pulse into the model prior to any reflections from the antenna arriving at the excitation interface (directly related to the number of time steps required to capture the model response). In this case there are alternative schemes that result in a reflectionless excitation plane, obviating the need for this large distance between feed plane and antenna.

REFERENCES

[1] D. M. Pozar, "Microstrip antennas," *Proc. IEEE*, vol. 80, pp. 79–91, Jan. 1992.
[2] T. Cwick and R. Mittra, "Scattering from a periodic array of freestanding arbitrarily shaped perfectly conducting or resistive patches," *IEEE Trans. Antennas Propagat.*, vol. AP-35, pp. 1226–1234, Nov. 1987.
[3] R. E. Jorgenson and R. Mittra, "Scattering from structured slabs having two-dimensional periodicity," *IEEE Trans. Antennas Propagat.*, vol. 39, pp. 151–154, Feb. 1991.
[4] D. T. McGrath and V. P. Pyati, "Phased array antenna analysis with the hybrid finite element method," *IEEE Trans. Antennas Propagat.*, vol. 42, pp. 1625–1630, Dec. 1994.
[5] E. W. Lucas and T. P. Fontana, "A 3-D hybrid finite element/boundary element method for the unified radiation and scattering analysis of general infinite periodic arrays," *IEEE Trans. Antennas Propagat.*, vol. 43, pp. 145–153, Feb. 1995.
[6] K. S. Yee, "Numerical solution of initial boundary value problems involving Maxwell's equations in isotropic media," *IEEE Trans. Antennas Propagat.*, vol. AP-14, pp. 302–307, May 1966.
[7] W. Tsay and D. M. Pozar, "Application of the FDTD technique to periodic problems in scattering and radiation," *IEEE Microwave Guided Wave Lett.*, vol. 3, pp. 250–252, Aug. 1993.
[8] J. Ren, O. P. Gandhi, L. R. Walker, J. Fraschilla, and C. R. Boerman, "Floquet-based FDTD analysis of two-dimensional phased array antennas," *IEEE Microwave Guided Wave Lett.*, vol. 4, pp. 109–111, Apr. 1994.
[9] W. L. Ko and R. Mittra, "Implementation of Floquet boundary condition in FDTD for FSS analysis," in *IEEE AP-S Symp. Dig.*, June 1993, pp. 14–17.
[10] P. Harms, R. Mittra, and W. Ko, "Implementation of the periodic boundary condition in the finite-difference time-domain algorithm for FSS structures," *IEEE Trans. Antennas Propagat.*, vol. 42, pp. 1317–1324, Sept. 1994.
[11] D. T. Prescott and N. V. Shuley, "Extensions to the FDTD method for the analysis of infinitely periodic arrays," *IEEE Microwave Guided Wave Lett.*, vol. 4, pp. 352–354, Oct. 1994.
[12] N. Amitay, V. Galindo, and C. P. Wu, *Theory and Analysis of Phased Array Antennas.* New York: Wiley, 1972.
[13] D. S. Katz, E. T. Thiele, and A. Taflove, "Validation and extension to three dimensions of the Berenger PML absorbing boundary condition for FD-TD meshes," *IEEE Microwave Guided Wave Lett.*, vol. 4, pp. 268–270, Aug. 1994.

Gregory M. Turner (M'96) received the B.E.E. degree from the Georgia Institute of Technology, Atlanta, in 1986, the M.Eng. degree from the University of Florida, Gainesville. in 1990, and the Ph.D. degree in electrical engineering from the University of Central Florida, Orlando.

Since 1986, he has been employed by Harris Corporation, Aerospace Systems Division, where his work involves the design, analysis, and measurement of antenna systems for space applications.

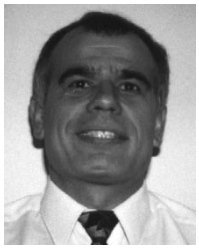

Christos Christodoulou (S'80–M'81–SM'90) received the B.Sc. degree in physics and mathematics from the American University of Cairo in 1979, and the M.S. and Ph.D. degrees in electrical engineering from North Carolina State University, Raleigh, in 1981 and 1985, respectively.

He served as a faculty member at the University of Central Florida, Orlando, from 1985 to December 1998. He is currently the Chair of the Electrical and Computer Engineering Department at the University of New Mexico, Albuquerque. He has more than 115 refereed journal publications and conference papers. His research interests are in the areas of modeling electromagnetic systems, neural network applications in electromagnetics, and smart antennas in wireless communications.

Dr. Christodoulou is a member of URSI (Commission B). He is also the General Chair of the APS/URSI 1999 Symposium in Orlando, FL. In 1991, he was selected as the AP/MTT Engineer of the year (Orlando section) and he served as the Secretary, Treasurer, and Vice President of the Orlando IEEE Section from 1995 to 1998.